Climate Dynamics (2019) 52:1903–1916
https://doi.org/10.1007/s00382-018-4268-2

Characteristics of northward propagating intraseasonal oscillation in the Indian summer monsoon

Nirupam Karmakar[1] · **T. N. Krishnamurti**[1]

Received: 17 November 2017 / Accepted: 26 April 2018 / Published online: 25 May 2018

Abstract
Indian summer monsoon exhibits strong northward propagation in intraseasonal timescale [intraseasonal oscillations (ISO)] from the equatorial Indian Ocean (EIO) to the foothills of the Himalayas. Initiation of this northward march is often marked by a strong convective activity over the EIO, which could be associated with Madden–Julian Oscillation. Satellite derived rainfall and reanalysis products are used to unravel different characteristics of ISO in terms of strength, extent and speed at different times. Eastern EIO convective events are grouped into two categories based on the intensities of the simultaneous rainfall anomalies over central India (CI). Northward propagation from EIO is observed to be much stronger and slower when CI experiences strong dry anomaly at the time of initiation of northward march of convection near the equator. Essentially, a first northward propagating dry lobe seems to impact the behavior of the next arriving wet lobe. Distinctive features in Rossby waves emanated from the eastern EIO and different surface and atmospheric conditions over the region in the two different cases are observed. Strong dry conditions over CI favors strong easterly vertical wind-shear, which eventually helps destabilizing the atmosphere. Upper tropospheric meridional temperature gradient over the region modulates the variation in vertical wind-shear via thermal wind balance. These conditions are favorable for generation of strong boundary layer convergence to the north of the convective band, producing strong northward propagation. These results indicate the dual role of convection near the equator and dryness over CI in modulating the northward march of rainfall over India.

Keywords Indian monsoon · Intraseasonal oscillation · Active and break spells · Northward propagation mechanism

1 Introduction

Indian region experiences one of the most pronounced and wide spread monsoon systems of the world (Gadgil 2003), which is associated with many global climatic features such as eastern Pacific sea surface temperature (SST) (Rasmusson and Carpenter 1983), northern Atlantic SST (Goswami et al. 2006) and Eurasian snow cover (Hahn and Shukla 1976). Indian monsoon has a far reaching impact over many parts of the globe, including the Arctic (Krishnamurti et al. 2015). Monsoonal floods and droughts leave an enormous socio-economic impact over more than a billion of inhabitants in the region. Thus, understanding monsoon dynamics and forecasting its behavior at different ranges has become one of the top-priority problems in weather and climate studies.

Indian summer monsoon rainfall possesses unique seasonal and intraseasonal characteristics. Intraseasonal rainfall is characterized by periodic spells of heavy rainfall (active spell) and low or less rainfall (break spell) (Yasunari 1980; Sikka and Gadgil 1980; Gadgil 2003; Rajeevan et al. 2010). This periodicity is initiated by certain oscillatory modes and exhibits wave-like structures called intraseasonal oscillation (ISO) (Krishnamurti and Subrahmanyam 1982; Webster et al. 1998; Annamalai and Slingo 2001; Goswami and Ajaya Mohan 2001; Krishnamurthy and Shukla 2007; Lee et al. 2013; Karmakar et al. 2017b). ISO waves are often linked with northward propagating convective bands (Yasunari 1979, 1980; Sikka and Gadgil 1980), which have a typical latitudinal scale of almost 30° (Chakraborty and Nanjundiah 2012). Krishnamurti et al. (1985) suggested that the

Electronic supplementary material The online version of this article (https://doi.org/10.1007/s00382-018-4268-2) contains supplementary material, which is available to authorized users.

✉ Nirupam Karmakar
nirupam.ju@gmail.com; nkarmakar@fsu.edu

[1] Earth, Ocean and Atmospheric Science Department, Florida State University, Tallahassee, FL 32306, USA

intraseasonal characteristics in the monsoon are likely to be modulated by a planetary-scale divergent wave that travels the globe in the eastward direction with a speed of almost 8° longitude/day. Many studies also noted that eastward moving Madden–Julian Oscillation (MJO) might play a role in the initiation of the northward march of convection from the equatorial Indian Ocean (EIO) (Madden and Julian 1972; Julian and Madden 1981; Lau and Chan 1986; Singh et al. 1992; Yoo et al. 2010; Pai et al. 2011). As ISO is governed by the internal dynamics (interaction between large-scale circulation and organized convection), predictability of monsoonal rainfall crucially depends upon the nature of ISO (Sperber et al. 2001; Rajeevan 2001). It was also noted that the potential predictability of ISO and error growth highly depend on the phases of ISO and MJO (Ding et al. 2011). Therefore, there is a need to advance our diagnostics on ISO and a better understanding of the dynamics of northward propagation and its connection with the equatorially trapped waves.

In this study, we aim to understand the nature of ISO as they evolve from the EIO and how they depend upon the atmospheric conditions over central India (CI). Typically, presence of convection over the EIO coincides with dry conditions over CI in the intraseasonal timescale (Krishnamurthy and Shukla 2007; Lee et al. 2013; Karmakar et al. 2017b). EIO convection often occurs with the arrival of a convective lobe of MJO over the region. Thereafter a northward march of convection occurs and in a matter of 15–20 days the convective band reaches CI. Here, we ask the following question: how the atmospheric conditions over CI modulates the behavior of the intraseasonal northward march of convection from the EIO? This study is an attempt to address this issue using observational analysis. The purpose of this study is to provide a better understanding on the diagnostic character of the strength and periodicity of ISO waves and how CI conditions modulate them. Similar issues were addressed in Moum et al. (2016) where they suggested stronger MJO pulses over the Indian Ocean are associated with lower cooling rates in the precedent pulse, thereby concluded that an MJO event is governed by the oceanic memory from the previous event. This memory effect might be useful in enhancing the predictive capabilities in intraseasonal timescale. Therefore, if information about the dry phase over CI provides some indication about the subsequent active spell, that would add value to the prediction of rainfall over the region. State-of-the-art models still have difficulties in simulating the behavior of monsoonal mean and variability. Short to medium-range forecast skills of the dynamical models critically depend on how they capture convection and its spatiotemporal variability (for example, ISO) (Rajendran et al. 2008). To this end, the results presented here could be used in model evaluation. Sections 2 and 3 provide descriptions of the the data used, and methodologies used in this study, respectively. Section 4 presents results of our simulations, followed by a discussions in Sect. 5.

2 Datasets

Tropical Rainfall Measuring Mission (TRMM) 3B42 (V7) daily rainfall data for 1998–2014 (Huffman et al. 2007) have been used for this study. Since we are interested in large-scale intraseasonal features, the data are re-gridded into 1°× 1° using bilinear interpolation for computational ease. Similar data and approach were made in Karmakar et al. (2017b).

European Centre for Medium-Range Weather Forecasts Re-Analysis (ECMWF) ReAnalysis (ERA)-Interim dataset (Dee et al. 2011) and the National Oceanic & Atmospheric Administration (NOAA) Optimum Interpolation Sea Surface Temperature (OISST) version 2 daily data (Reynolds et al. 2007) are also used for the same period (1998–2014). Different fields from reanalysis data (e.g., mean sea-level pressure, winds, temperature, specific humidity and geopotential height) are obtained and daily averaging is done from the 6-hourly data. All the fields are converted to 1°× 1° resolution before analysis.

3 Methodology

A data-adaptive filtering technique, namely multichannel singular spectral analysis (MSSA) (Plaut and Vautard 1994; Ghil et al. 2002) has been performed on the rainfall data over the south Asian monsoon domain (10°S–35°N and 60°E –110°E). After removing the daily climatology at each grid point from the 17-year data and pre-filtering it with a 5-day moving mean to remove very high-frequency fluctuations, an extended monsoon period (May–October) is taken and fed into MSSA algorithm.

MSSA has been used extensively in the last few decades to understand and analyze spatiotemporal behavior of short and noisy time series. The advantage of MSSA compared to other harmonic analyses or fast Fourier analysis is that the shape and bandwidth of the filters in MSSA are functions of the input data itself. The technique is very useful in capturing anharmonic oscillations arising from nonlinear phenomena. A lag-covariance matrix, constructed by augmenting lagged copies of the data, is diagonalized to obtain space-time empirical orthogonal functions (ST-EOFs) and temporal principal components (ST-PCs). An oscillation is present in the data if the phase of two ST-EOFs are in quadrature and the associated eigenvalues are almost equal (Plaut and Vautard 1994). Following Allen and Robertson (1996), we used a statistical test with 1000 red-noise surrogates to prevent any random fluctuation and noise being treated as

an oscillatory mode. Only significant oscillatory modes that capture oscillations with a periodicity of 20–60 days are used to reconstruct the data. The reconstruction is defined as low-frequency ISO for each year. ISO time series is of the same length as of the input data (184-days). The same approach was adopted in Karmakar et al. (2017b) and intrinsic features of ISO were captured (see their Fig. 3). ISO-filtered time series averaged over CI approximately represents the active-break cycle of rainfall over the region. We refer to Karmakar et al. (2017b) for further methodological details.

We also make use of t-statistic to test the statistical significance of various results presented in our study.

4 Results

4.1 Northward propagation: strong and weak dry cases

ISO-filtered time series averaged over the eastern EIO (5°S –5°N and 85°E– 95°E) for May–October every year is used as a reference to study the evolution of northward propagation from the EIO. This time series is then normalized, and the dates when the anomalies exceed +1-standard deviation are determined. We mark the first day (lag-0) as a reference date of this multiple-day period when this threshold is met. This is done for all the 17 monsoon seasons from 1998–2014 individually. There are 55 such events in this 17-year period. In Fig. 1a, composited rainfall anomalies during such events (compositing all days when ISO-filtered

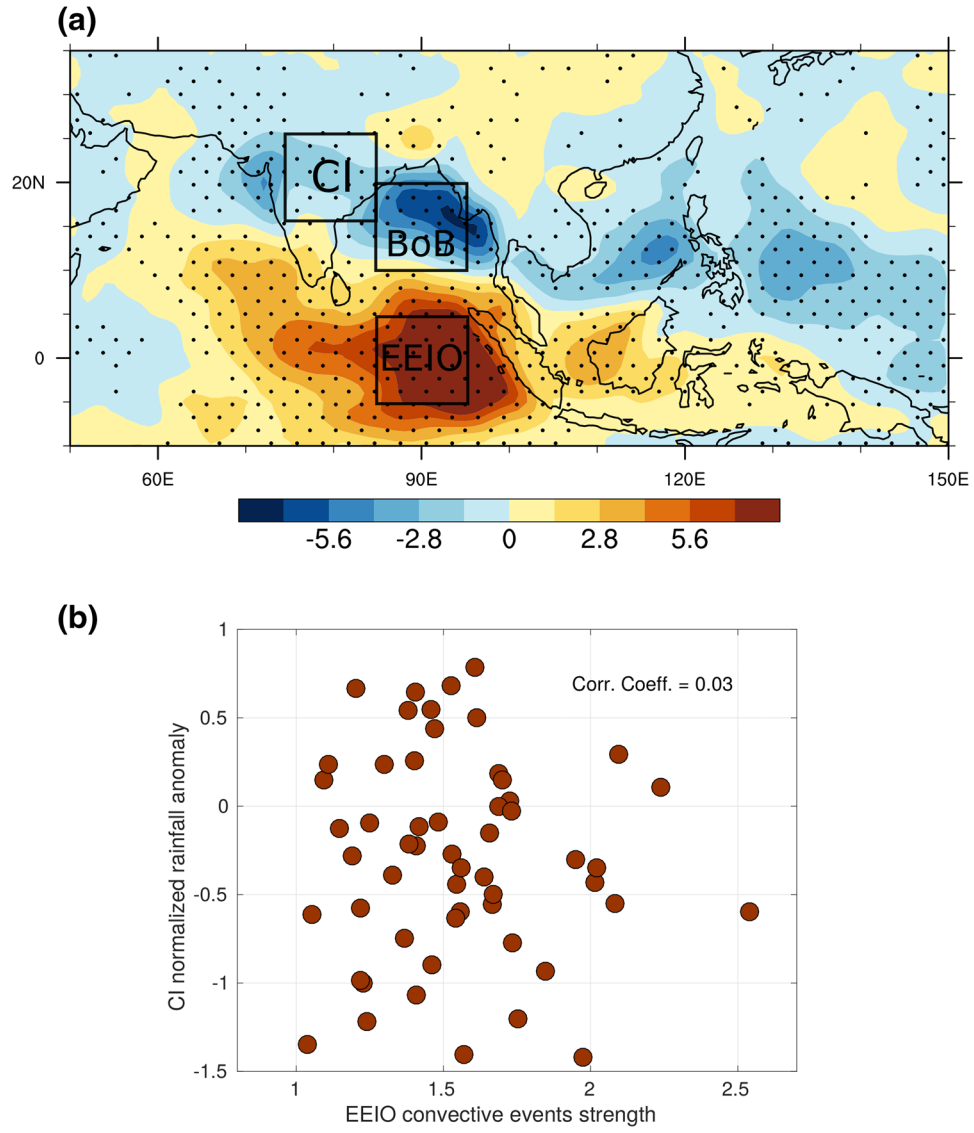

Fig. 1 **a** Composited rainfall anomalies (mm/day) for the events when the normalized eastern EIO (5°S–5°N and 85°E –95°E) ISO exceeds + 1-standard deviation. Boxes indicate the eastern EIO, CI and BoB regions taken for analysis. Dotted areas indicate the regions where the mean is significantly (at 1% level) different from 0. **b** Scatterplot of normalized eastern EIO ISO values during the convective events over eastern EIO and normalized CI (16°N –26°N and 75°E–85°E) rainfall anomalies

rainfall anomalies averaged over the eastern EIO exceeds + 1-standard deviation) are shown. Clearly, a strong positive rainfall anomaly is located over the eastern EIO region. A negative rainfall anomaly is located over the central Indian region. This resembles the typical break-like conditions over CI (Rajeevan et al. 2010; Karmakar et al. 2017b).

To investigate the possible role of CI dryness in modulating northward ISO propagation, we average the rainfall anomalies (no filtering is done) over CI (16°N–26° N and 75°E–85°E) and normalize for individual seasons. Figure 1b shows the scatter-plot of the values of ISO-filtered rainfall over the eastern EIO versus the simultaneous normalized CI rainfall anomalies for the 55 convective events identified over the eastern EIO. Although the composite in Fig. 1a shows the negative values over India, there exists a large spread in the rainfall anomaly over CI when there is a strong wet condition over eastern EIO (correlation value is − 0.03). However, most of the CI values show negative sign, which contribute to the negative values in the composite figure. This large spread in CI rainfall anomaly suggests that the dryness over CI may not be strongly coupled to the convection anomaly over eastern EIO.

These 55 convective events over the eastern EIO are categorized based on the dryness over CI. We define strong dry events over CI when normalized CI rainfall anomaly is below − 0.5 and weak dry events as when the value is more than 0. Weak dry events essentially represent the case when CI experiences some rainfall, possibly arising from synoptic variability or extreme rain events, when the dry ISO lobe is present over the region. There are 20 strong dry events and 18 weak dry events identified. The aim is to understand the contrast between the strong and weak dry events, which would provide us an idea on how CI conditions might modulate the nature of the subsequent northward propagating wet lobe of ISO. In Fig. 2a, b, composites of the time–latitude diagrams of 85°E–90°E averaged vertically integrated moist static energy (MSE; defined as the sum of potential, internal and latent energy of an air parcel) and rainfall anomalies for the strong and weak dry events are shown, respectively. The rainfall anomalies are well consistent with vertically integrated MSE anomalies and both the fields exhibit strong northward propagation. Propagation is seen in both the strong and weak dry cases. Northward movement in MSE anomalies indicates the role of intraseasonal northward propagation in carrying energy/heat content towards India from the EIO. Clearly, in the strong dry case, northward propagation is much more prominent and stronger than in the weak dry case. Also, the eastern EIO convection exhibits stronger magnitude and larger extent when CI is drier. Positive MSE anomalies show propagation upto 35°N from the equator in the strong dry case, whereas, the northward march is limited to 25°N in the weak dry case. The rainfall anomaly maxima in the Indian land is located farther north in the strong dry case (19°N) compared to weak dry case (14°N). Propagation speed is comparatively slower during the strong dry case (1° latitude/day) than in the weak dry case (1.5° latitude/day). Also, in strong dry case the positive anomalies started showing northward propagation from more south of the equator compared to that in weak dry case. This suggests that not only the eastern EIO convection in low-frequency intraseasonal timescale modulates the northward propagation over India, but also the dryness over CI has a large role to play in the strength and speed of the intraseasonal variability in convection.

Naturally, one can ask how these northward propagation with different characteristics impact the actual rainfall over India. To understand this, we averaged the total rainfall over the CI region during each event and composited for strong and weak dry cases (Fig. 2c). During lag-0 the total rainfall over CI is lesser in the strong dry case than in the weak dry case, which is as expected. After lag-13, the amount of rainfall over the CI shows much larger values during the strong dry case compared to the weak dry case. Now, the nominal time taken by convective bands to reach CI from the EIO region is also nearly half-a-month. Which indicates the total rainfall also exhibits strong intraseasonal features during the strong dry case. Therefore, the phase of convection over the eastern EIO and the dryness over CI could possibly lead us to understand the rainfall variability in active-break spells over CI. Which has a large implication to the probabilistic estimation of rainfall over the region.

Similar to CI, analysis considering a region over the Bay of Bengal (BoB) (10°N–20°N and 85°E–95°E) is also performed to further examine the robustness in our results and are presented in the Supplementary Information (SI). Normalized rainfall anomalies over BoB shows a stronger negative correlation (− 0.27) with convection over eastern EIO. Defining dry events based on the BoB box results 33 strong dry and 9 weak dry cases (Figure S1). Large difference in the number of strong dry case based on indices over the CI and BoB regions suggests the dynamics of ISO could be different over the land compared to oceans. However, in both the analyses, strong dry case exhibit slower propagation rate with higher intensity than in the weak dry case.

4.2 Distinctive features in the two cases: Rossby waves

In Fig. 3a, b, the lower tropospheric wind and mean sea-level pressure anomalies composited for the two cases are shown. Rossby wave emanation from equatorial convection is seen in both the cases. But it observed to be weaker in amplitude in the weak dry case. In lag-0, a Rossby wave response to convective heating is seen as was predicted by Gill (1980). Rossby lobes are present in both the hemispheres (marked by *R* in the maps in the north hemisphere, which are stronger

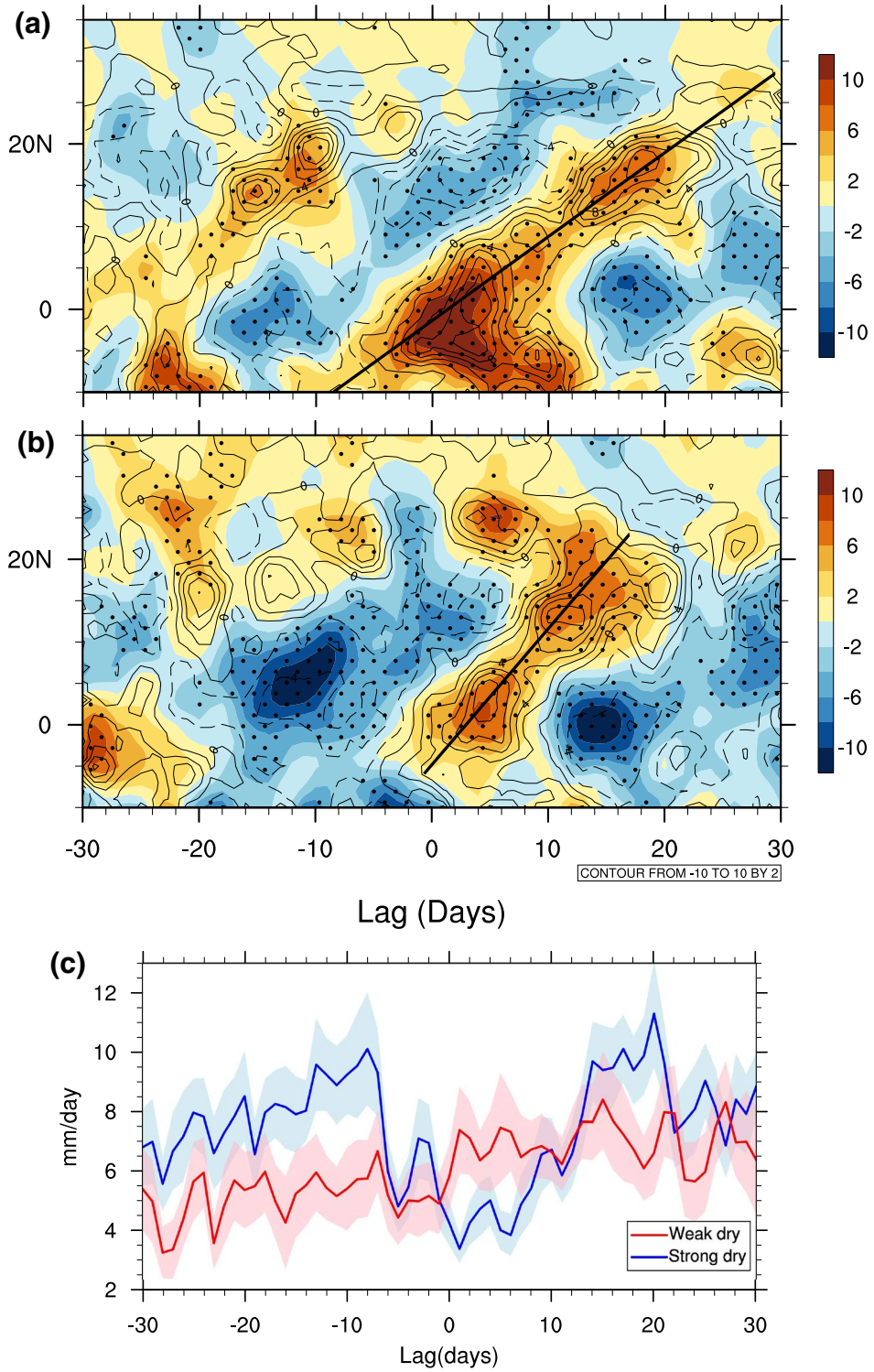

Fig. 2 **a** Time–latitude diagram of composited vertically integrated MSE (shaded; in $\times 10^{-6}$ J/m^{-2}) and rainfall (contours; in mm/day) anomalies averaged between 85°E and 90°E during strong dry cases. **b** Same as **a**, but for weak dry cases. Solid (dashed) lines represent positive (negative) rainfall anomalies and the contours are given from − 10 to 10 with an interval of 2 mm/day. Solid staright lines indicate northward propagation. Dots mark the places where the mean vertically integrated MSE is significantly (at 10% level) different from 0. **c** CI averaged rainfall during strong and weak dry cases. 0-th day is the first date in each multi-day period when ISO associated rainfall over eastern EIO exceeds + 1-standard deviation. Shaded areas indicate the spread of the values around the mean at each lag-day, normalized by the number of samples

than in the southern hemisphere) and by lag-5 the northern hemisphere lobe moves northward and westward. Subsequently, another lobe forms over the Sumatra coast and both the lobes propagate northwestward by lag-10. By lag-15, the first lobe reaches northern Arabian Sea and weakens and the second lobe moves towards CI. In subsequent days, this second lobe reaches CI and weakens over the foothills of the Himalayas within few days.

The strong anomalous anticyclonic flow with strong positive mean sea-level pressure anomaly seen on lag-0 over CI in the strong dry case, is virtually absent in the weak dry case. This circulation pattern is associated with weaker

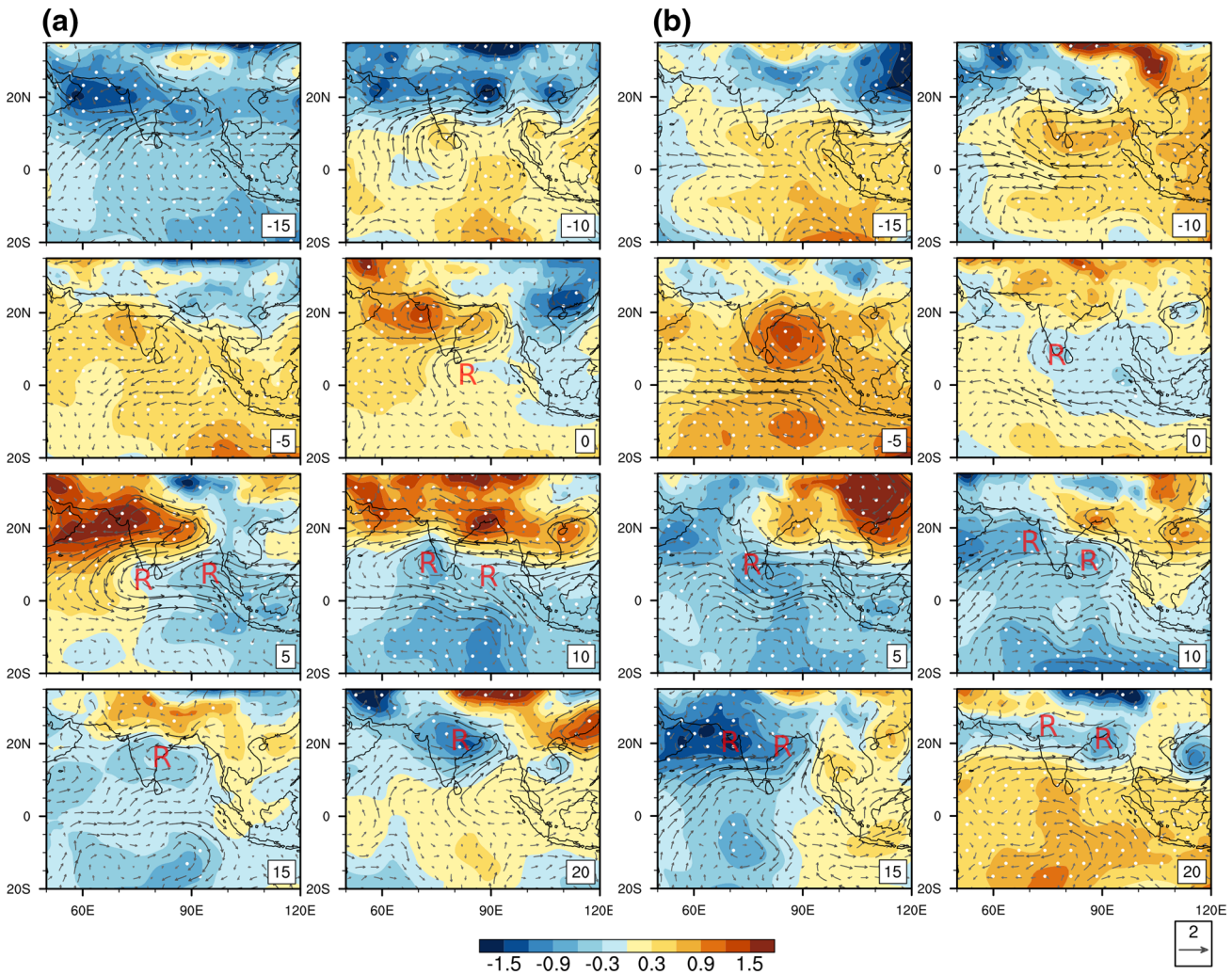

Fig. 3 **a** Mean sea-level pressure (shaded; in hPa) and lower tropospheric (850 hPa) wind (vectors; in m/s) anomalies for strong dry cases. **b** Same as **a**, but for weak dry cases. *R* indicate location of the Rossby lobes. Numbers in each panel indicate the lag (in days). White dots indicate the regions where the mean is significantly (at 10% level) different from 0

break-like situation over CI in lag-0 when convection is set over eastern EIO in the weak dry case. Generation of Rossby waves in response to convection over EIO is observed, but the propagation speed of the Rossby lobes is faster in the weak dry case compared to the strong dry case. Northern hemisphere Rossby cells show larger and stronger anomalies than in the southern hemisphere. Nature of Rossby waves in the context of Indian monsoon was previously documented in Kemball-Cook and Wang (2001) amongst few others. The overall characteristics of the Rossby lobes are substantially linked with the mean easterly vertical shear in the northern hemisphere (Xie and Wang 1996), which also confines the Rossby wave to response stronger in the lower tropospheric levels compared to the upper level. We also observe Rossby wave propagation of low-level anticyclonic lobe (associated with suppressed convection) from the BoB towards India during lag-(-10) to lag-0. This propagation is more pronounced in the strong dry case. This supports the findings in Krishnan et al. (2000), where they suggested breaks over CI are initiated by the arrival of convectively stable anomalies traveling from central BoB towards India. These anomalies are marked by abrupt Rossby wave movement and reach CI within a matter of few days.

In Fig. 4a, b, we show skin temperature and 1000 hPa level specific humidity anomalies at different lags. For the strong dry case, in lag-(-5) a strong positive skin temperature anomaly is developed over the peninsular India along with a negative specific humidity anomaly. These anomalies propagate northward and westward at lag-0 and create a strong warm and dry environment over CI associated with a strong break condition. In subsequent days, the anomaly structures propagate further northwestward. It is also seen that the center of convergence associated with the Rossby lobe in the northern hemisphere moves in conjunction with negative

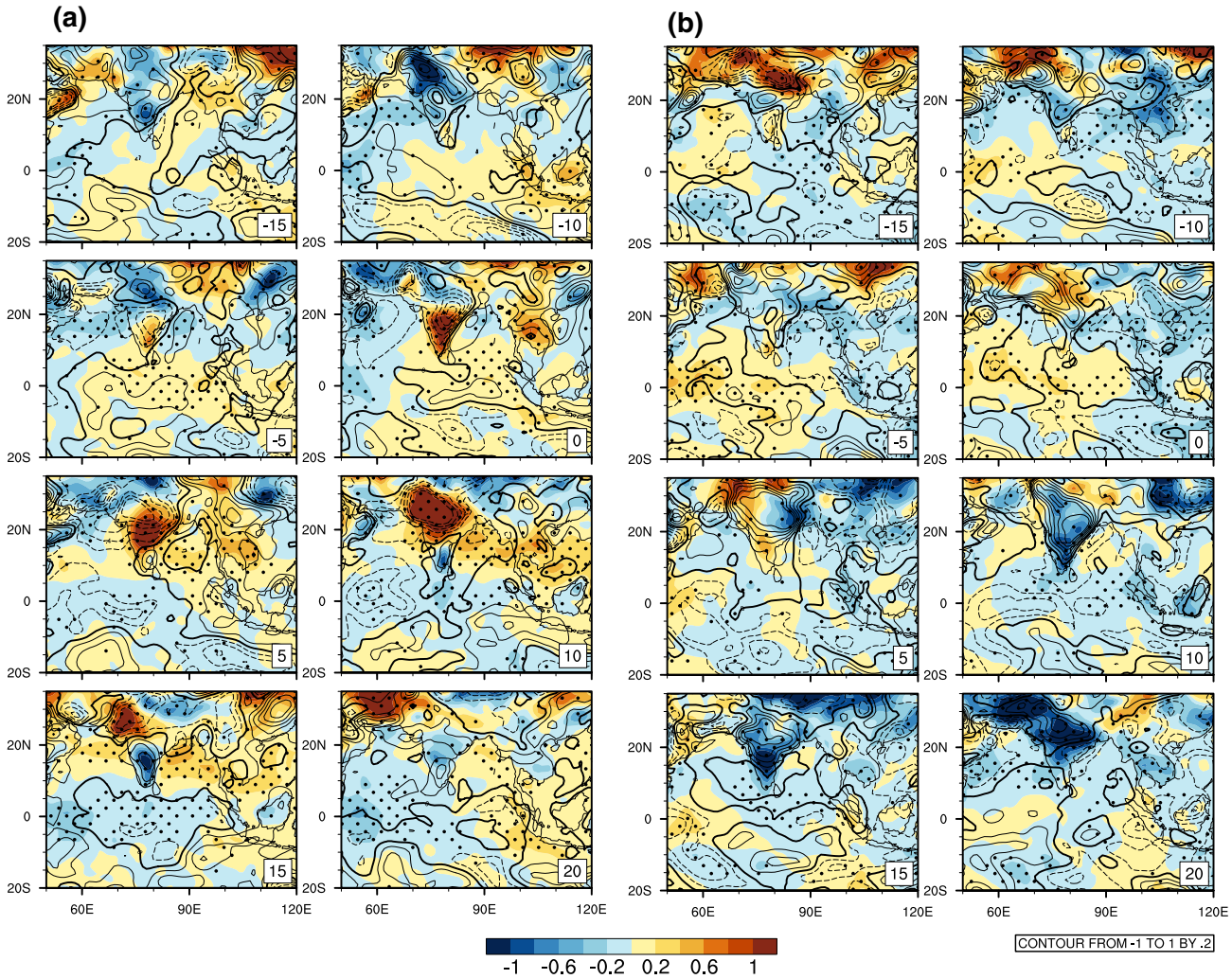

Fig. 4 **a**, **b** Same as Fig. 3a, b, respectively, but for skin temperature (shaded; in K) and 1000 hPa specific humidity (contours; in g/kg) anomalies. Negative specific humidity anomalies are shown in dashed contours. Dots indicate the regions where the mean of skin temperature is significantly (at 10% level) different from 0

skin temperature and positive specific humidity anomalies. However, the scenario is quite different in the weak dry case. Skin temperature anomalies do not show strong signatures over the CI during lag-0, possibly associated with the positive rainfall anomalies over CI (as defined) at the same time. Strong dry case is associated with a persistent positive skin temperature anomaly over the eastern EIO during lag-(-10) to lag-0, which is not seen in the weak dry case.

Frictional convergence plays a major role in northward propagation of ISO. Cyclonic vorticity associated with the Rossby lobes drives the planetary boundary layer frictional convergence, which leads to higher moisture content to the north of the convection center (Xie and Wang 1996). This helps the convection to move northward. Therefore, the specific humidity anomalies at 1000 hPa could play a major role in the northward propagation of convection. These anomalies are markedly different in the two cases. The strong dry case is witnessed by positive anomalies associated with the Rossby lobes, amplifying the convergence. In contrast, the surface humidity over eastern EIO in lag-0 is weaker in the weak dry case than in the strong dry case. Surface specific humidity associated with the Rossby lobes as seen in lags-0 and 5 are of smaller magnitude in the weak dry case. Which suggests that the moisture convergence associated with the cyclonic vorticity is weaker in the weak dry case. A point to note here, there is a strong positive specific humidity anomaly located over CI during the weak dry case at lag-0, compared to a negative anomaly in strong dry case. This positive anomaly is again linked with the positive rainfall anomaly over CI as defined for the weak dry case. Indian land exhibits

anomalously strong positive specific humidity values in almost all the phases of weak dry case ISO propagation.

Positive skin temperature anomalies along with surface humidity anomalies of the same sign over eastern EIO during and before lag-0 in the strong dry case suggests the presence of strong equatorial convection. This is more prominent in Fig. 5, where SST shows persistent positive anomalies during lags-(-10),(-5) and 0 in the strong dry case. Steady positive SST anomalies are associated with strong equatorial convection, which enforces the meridional overturning circulation (Hadley cell) as seen from the 500hPa level vertical wind structures. Strong upward vertical motion is seen during lags-0 to 10 over the eastern EIO. The descending branch of the Hadley cell over CI forces strong dry conditions over

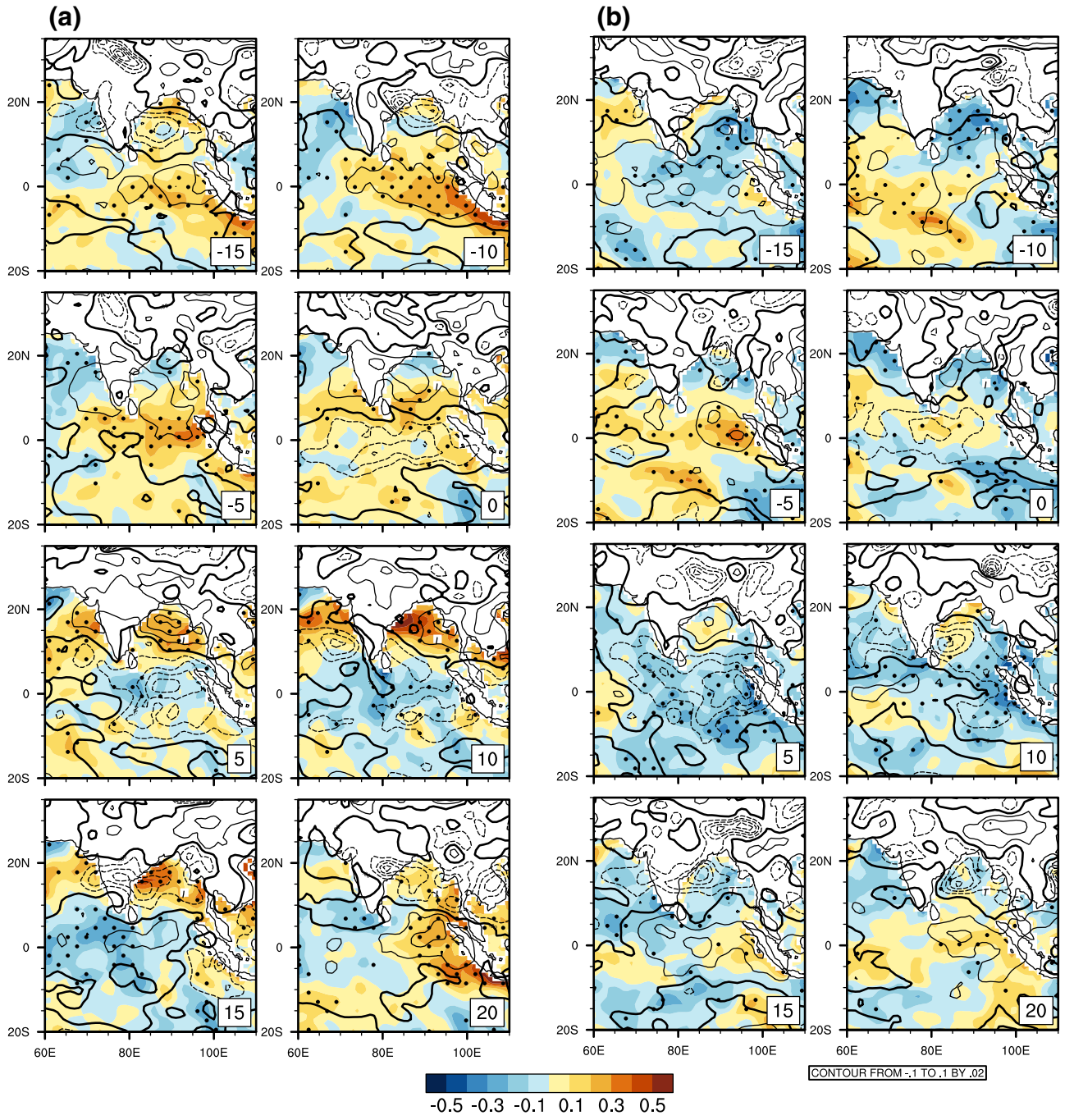

Fig. 5 **a**, **b** Same as Fig. 3a, b, respectively, but for SST (shaded; in K) and 500hPa vertical winds (contours; in Pa/s and positive implies downward motion) anomalies. Downward motion is shown in dashed contours. Dots indicate the regions where the mean of SST is significantly (at 10% level) different from 0

the region. This persistence in SST and well structured Hadley cell are absent in the weak dry case. We note here that the stronger negative MSE anomaly over the EIO in the weak dry case during lag-(-10) (Fig. 2) could be related with less persistent positive SST anomalies. Weaker positive SST anomalies could give rise to decreased surface fluxes, which can result into decrease in vertically integrated MSE in the weak dry case. Seo et al. (2007) suggested that the surface meridional moisture convergence is a key factor for northward propagation of convection. Improving basic state SST, winds and vertical shear could markedly enhance the representation of ISO in numerical simulations. To this end, better understanding of the relationship between convection and these key parameters is needed for further development of ISO prediction.

4.3 Vertical shear and stability of the atmosphere

An alternate mechanism for northward propagation of ISO, which takes into account the vertical wind shear over the Indian region is also examined for different northward propagating ISO events (Jiang et al. 2004). Wang and Xie (1997) also noted the role of mean easterly vertical shear in amplifying northern hemisphere Rossby lobes. In Fig. 6a, absolute values of vertical shear of wind averaged over CI is plotted against the lag days for the strong and weak dry cases.

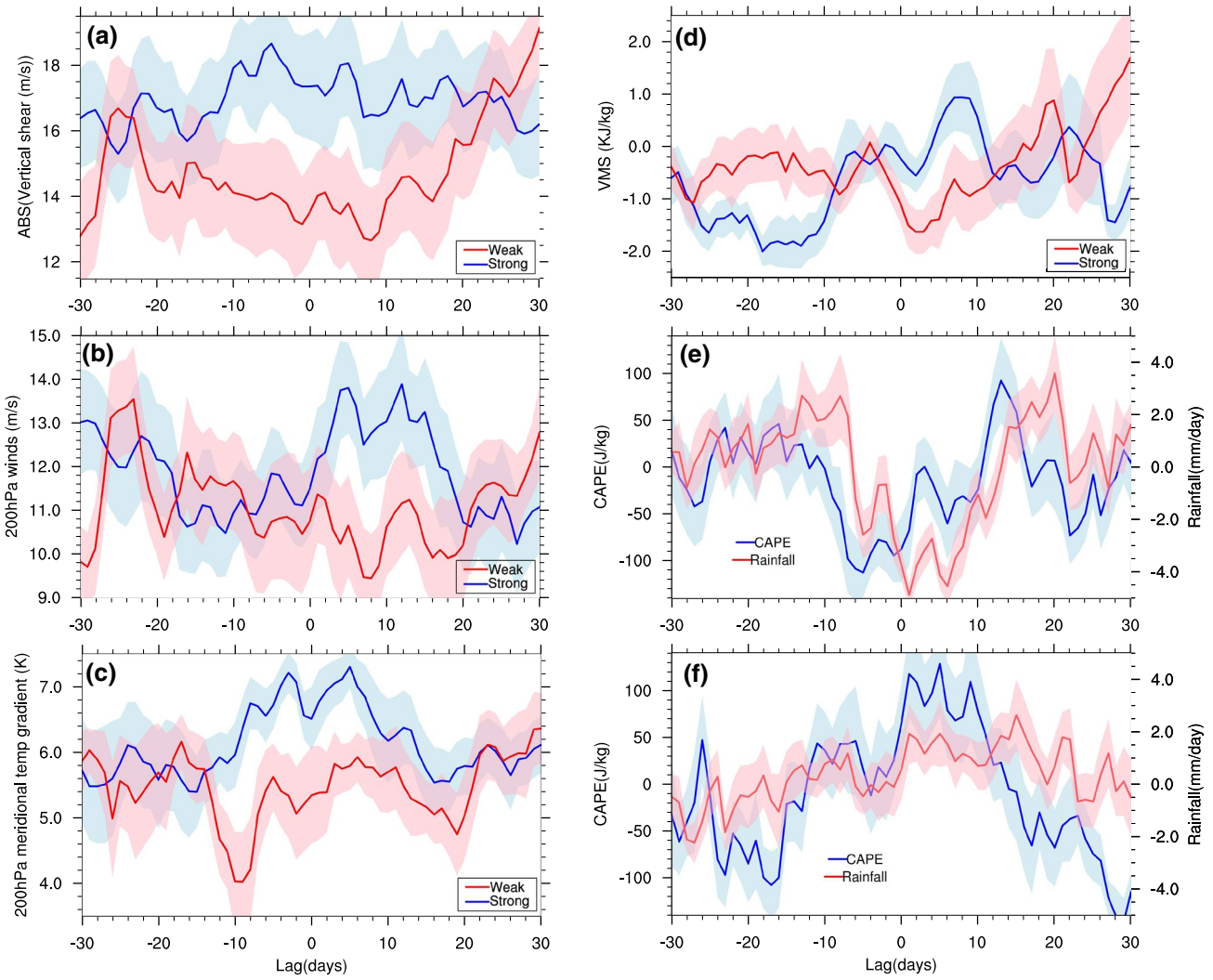

Fig. 6 **a** Area averaged composited vertical shear ($U_{200hPa} - U_{850hPa}$; in m/s) in absolute values over the CI region as a function of days (in lags). *x-axis* is same as in Fig. 2c. **b** Same as **a**, but for U_{200hPa} in absolute values over CI. **c** Same as **a**, but for 200 hPa meridional temperature gradient over India calculated based on the difference in temperature over a box over Tibet (30°N–35°N and 80°E–90°E) and the other over the EIO (2°S–3°N and 75°E–85°E). **d** Same as **a**, but for vertical moist stability (VMS; equals to $MSE_{top} - MSE_{bottom}$, with middle defined as 600 hPa; in kJ/kg) over CI. **e** Area averaged composited convective available potential energy (CAPE, left *y- axis*; in J/kg) and rainfall (right *y-axis*; in mm/day) anomalies for strong dry case over CI. **f** Same as **e** but for weak dry case. Similar to Fig. 2c, shaded regions show the spread of the values around the mean at each lag day

Vertical shear over CI shows persistently stronger behavior in the strong dry case and exhibits a maxima at lag-(-5). This strong easterly shear gives rise to the generation of barotropic vorticity to the north of the convection center, which in turn leads to the genesis of barotropic divergence in the free atmosphere. This helps for boundary layer convergence to the north of the existing convection (Jiang et al. 2004). Difference in the vertical shear in the two case arises from the difference in the strength of the 200 hPa level wind after lag-0 (Fig. 6b). During lag-5 to lag-15 upper level winds are persistently roughly 4 m/s stronger in the strong dry case as compared to weak dry case, which contributes to the difference in the vertical shear.

Why does the 200 hPa level wind shows this marked difference? Primary mechanism that maintains the upper level easterly jet over India arises from the thermal wind balance, which depends upon the meridional temperature gradient over the region. Two boxes are taken to determine this temperature gradient, one over Tibet (30°N–35°N and 80°E–90°E) and the other over the EIO (2°S–3°N and 75°E –85°E). 200 hPa air temperature difference between these two boxes provides an estimate of the meridional temperature gradient over India. Strength of the upper level jet is proportional to this temperature difference. It is observed that the strong dry case witness nearly 2K higher temperature difference than that in the weak dry case (Fig. 6c). This difference sustains for almost 2 weeks spanning from lag-(-7) to lag-7. This enforces the upper level jet to be much stronger over India during the active spell resulting into enhanced convection. As the convection sets in over CI, vertical wind shear weakens (after lag-10). In contrast, the weak dry case shows weaker signature of vertical wind shear during and before lag-0. In fact, the vertical shear in the weak dry case shows a minima during lag-0 to lag-(-10). This could be related to the positive rainfall anomalies over CI at that time in weak dry case (by definition), possibly arising from small-scale synoptic disturbances, which weakens the vertical shear of winds over the region. An increase in the vertical shear can be seen after lag-10 in the weak dry case.

Vertical wind shear plays an instrumental role in the initiation and evolution of northward march of ISO. Development and maintenance of convective bands require further favorable atmospheric conditions, for example, the large-scale stability of the atmosphere. The stability of the atmosphere can be examined by defining vertical moist stability (VMS) of an atmospheric column. VMS is defined as the difference between the vertically integrated MSE of the top and the bottom of the atmosphere ($MSE_{top} - MSE_{bottom}$) (Neelin and Held 1987). Increase in VMS would indicate stability of the atmosphere. VMS below a certain threshold provides a necessary condition for the existence of deep convective cloud structures (Srinivasan and Smith 1996). In Fig. 6d, we show VMS averaged over CI for both the cases. It is seen that the VMS values are higher in strong dry case during lag-0 to lag-10, indicating that CI possesses more stable atmosphere during break-spell in the strong dry case compared to weak dry case. However, after lag-10, stability in the strong dry case drops quickly and remains lower compared to the weak dry case.

The convective available potential energy (CAPE) is also a good indicator of atmospheric stability and a measure of the positive buoyancy of air parcel. CAPE is computed by integrating vertically the buoyancy of an air parcel from the level of free convection to the equilibrium level. For both the strong and weak dry cases, CAPE is computed over the CI region and it is found that the CAPE shows a strong relation with the rainfall anomalies over CI for strong dry case (Fig. 6e). CAPE over CI attains minimum value during a week before lag-0. Within a few days, CAPE builds up over CI and in 10–12 days after lag-0 it attains maxima in the strong dry case. The rainfall pattern follows the same variability but with a lag of roughly a week. Rainfall maxima over CI is observed at lag-20, as we already seen from Fig. 2c. This is consistent with the idea of development of CAPE before deep convection occurs. Negative CAPE anomalies near lag-0 in the strong dry case is consistent with the fact that the meridional overturning circulation over the region is stronger in this case and the descending branch of Hadley cell suppresses convective activity (Fig. 5a). Slow and steady development of CAPE is associated with northward march of SST anomalies. Strong persistent SST anomalies over the EIO and Hadley cell structure during and before lag-0 are consistent with the CAPE values over CI. This study also indicates the lead-lag relation (of roughly a week's timescale) of CAPE and precipitation. Phase relation between convection and precipitation at diurnal timescale has been studied in the Indian summer monsoon context (Subrahmanyam et al. 2015). But this relationship within the intraseasonal timescale has never been documented before. These findings would provide new insight on the stability of the atmosphere and convection which is essential for convective parameterization in dynamical models predicting rainfall over India.

In the weak dry case, this lead-lag relationship is not pronounced and higher CAPE values are present over CI during and just after the phase when convection is located over eastern EIO (lag-1 to lag-10) (Fig. 6f). This increased value in CAPE is associated with the positive rainfall anomalies over CI in the weak dry case. Possibly these atmospheric conditions in terms of higher values of CAPE favors faster propagation rate for weak dry case compared to the strong dry case. However, CAPE sharply diminishes after lag-10 making the CI atmosphere less favorable for deep convection. Thus, the intraseasonal wet lobe in the weak dry case experiences a more stable atmosphere with lesser CAPE values than in the strong dry case. In spite of the presence of

higher surface specific humidity anomalies, this essentially reduces rainfall anomalies over CI in active spell in the weak dry case.

Similar analysis over the BoB shows stronger intraseasonal character in the strong dry case (Figure S6). However, vertical shear, VMS and CAPE show much weaker variability during the intraseasonal passage over BoB as compared to over land in CI.

5 Summary and discussions

In this study, we demonstrate that the nature of northward propagation of convective bands from the EIO region in intraseasonal timescale could depend on the previous dry phase over CI. We classified northward propagating convective ISO events from the EIO region into two categories based on the strength of the simultaneous dry lobe over the central Indian region. Strong dry events are those when strong convection over EIO in the intraseasonal timescale coincides with strong dry anomaly over CI. Our analysis suggest that stronger dry phase over CI leads to slower and stronger low-frequency intraseasonal variability in rainfall anomalies. Northward march of ISO is also stretched into a larger meridional extent in the strong dry case. In other words, if a dry lobe arrives with a large amplitude over central India, it is noted that it impacts the next wet lobe, whose arrival over central India ends up with large rains. Different atmospheric conditions, for example, surface humidity, easterly vertical wind shear, and stability of the atmosphere possibly play crucial role in determining the northward march of convective bands from the equatorial Indian Ocean.

Strong dry conditions over CI co-exists with stronger easterly vertical shear, which may eventually destabilize the atmosphere and builds up CAPE in a matter of few days. These conditions are favorable for the generation of boundary layer convergence to the north of the convection. Also, the skin temperature and near surface specific humidity anomalies over the region are favorable in generation and propagation of Rossby waves from eastern EIO. Moisture convergence along with cyclonic vorticity is seen over the Indian region in strong dry case. Our results are consistent when the northward propagating ISO behavior is examined based on a box over BoB instead of CI (Figures S1–S7 in the SI). This study further warrants sensitivity model tests to verify the results found in our work.

Convection over the eastern EIO in intraseasonal timescale is highly modulated by MJO and there are few studies that showed links between the Indian monsoon rainfall and MJO phases (Pai et al. 2011). We also find similar results in our study, which shows a strong correspondence between the MJO phases and convection over the eastern EIO and CI. Figure 7a shows composite rainfall anomalies in the different phases of MJO (as defined in Wheeler and Hendon (2004)) over 1998–2014. Phases 1–3 corresponds to strong positive rainfall anomalies over the eastern EIO. Negative rainfall anomalies over CI are strongest during phase 1.

To understand better how the eastern EIO and CI rainfall are linked with the MJO phases, we calculated the number of days when ISO-filtered rainfall anomalies over these regions are more/less than + 1/− 1 standard deviation and estimated how these days are distributed within the 8 MJO phases (Fig. 7b–e). It is observed that nearly 60% of the days when ISO-filtered rainfall anomalies over the eastern EIO is more than + 1-standard deviation coincide with MJO phases 1 and 2. These phases are also when CI witness dry conditions, indicating the possible link between MJO and intraseasonally varying signal over the region. The association is stronger when the MJO is strong. Phases 5 and 6 are favorable for eastern EIO dry ISO phase, and almost at the same time (phases 4 and 5) wet conditions associated with ISO are observed over CI. Results are consistent when we perform analysis considering the box over BoB (Figure S7).

In spite of the fact that we calculated the rainfall ISO in our analysis in a completely different way than the MJO indices were produced in Wheeler and Hendon (2004) using OLR and zonal wind datasets, MJO phases and ISO over the south Asian region shows strong association and suggests that the two signals might not be physically independent. Understanding the actual physical mechanism on how eastward propagating MJO and northward propagating ISO are linked requires meticulous observational analysis and numerical modeling.

The results presented here also supports previous findings on decreasing strength of ISO variability over India in recent decades (Karmakar et al. 2015, 2017a). This decrease is associated with an increase in the number of extreme rain events in the monsoon season, especially during the break phase over CI. Increased extreme rainfall events tend to reduce the easterly vertical shear and stabilize the atmosphere during the subsequent active phase (Karmakar et al. 2017a). Low pressure systems (LPS) originating from the BoB, which are often linked with extreme rain events are strongly modulated by the large-scale circulation associated with intraseasonal variability (Goswami et al. 2003; Krishnamurthy and Ajayamohan 2010; Karmakar et al. 2015). Active spells are characterized by a significantly increased number of LPS as compared to break spells. It was shown that the increase in the extreme rain events over CI are closely associated with an increase in weak LPS (Ajayamohan et al. 2010). Although it is speculative at this point, increased extreme rain events can decrease the strength of the dry spell over CI. This might lead to weaker active phase rainfall and eventually lesser seasonal mean. A study on how LPS/extreme rain events contribute to the two different cases of active spells over CI described in this study could lead us

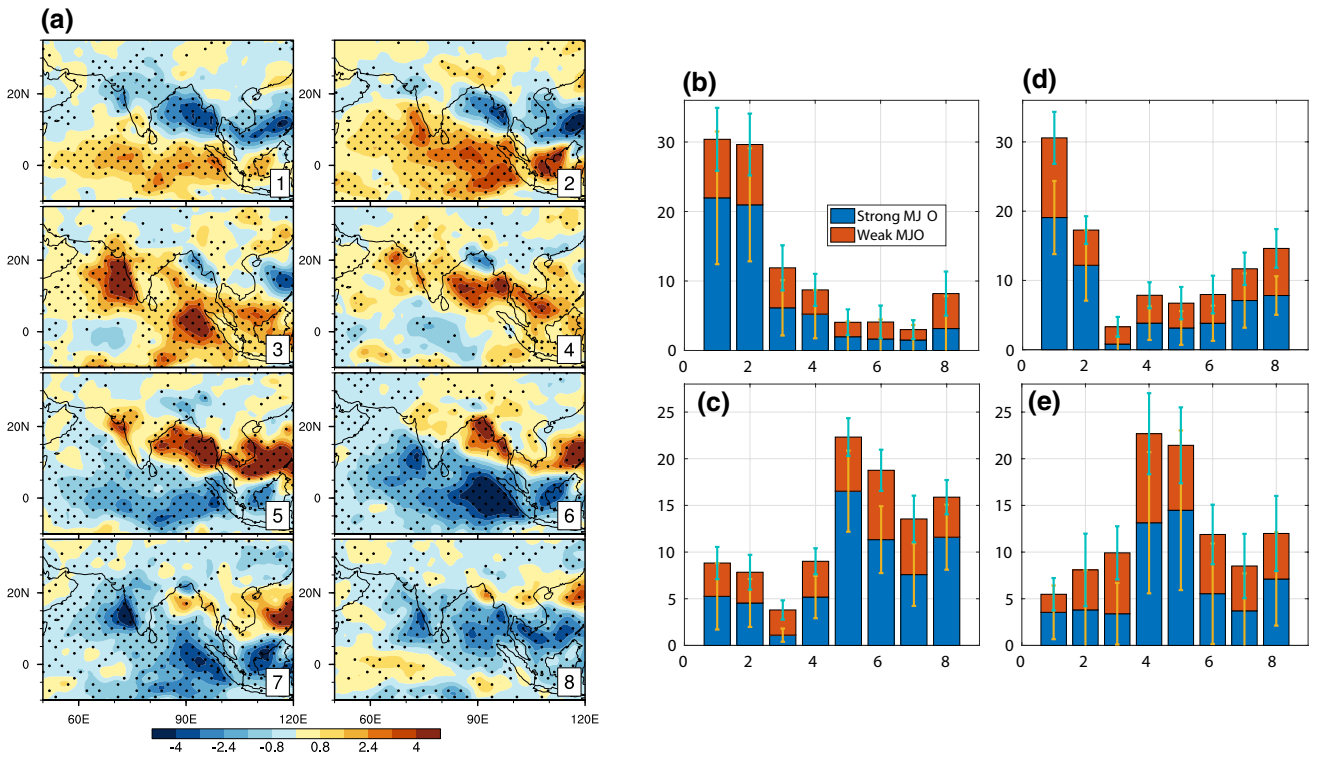

Fig. 7 **a** Composited May–October rainfall anomalies (mm/day) for different phases of MJO (based on Wheeler–Hendon index) during 1998–2014. Dots indicate the regions where the mean is significantly (at 5% level) different from 0. **b** Percentage of days when rainfall anomalies associated with ISO over eastern EIO exceedes + 1-standard deviation in different phases of MJO. **c** Same as **b**, but for days when rainfall anomalies associated with ISO over CI are below − 1-standard deviation. **d** Same as **b**, but for days when rainfall anomalies associated with ISO over eastern EIO are below − 1-standard deviation. **e** Same as **b**, but for days when rainfall anomalies associated with ISO over CI are above + 1-standard deviation. Errorbars show 10% confidence intervals on the calculated means. Refer to Wheeler and Hendon (2004) on how MJO strength and phases are calculated. Data for MJO indices are obtained from http://www.bom.gov.au/climate/mjo/graphics/rmm.74toRealtime.txt

to better understand the mechanics of active-break cycle in a warming climate.

There has been a lot of debate on how the Indian summer monsoon rainfall might change in the background of increasing SST and moisture, and enhanced greenhouse gas emissions (Turner and Annamalai 2012; Sharmila et al. 2015). However, weakening large-scale circulation over the region could act in a different way to change the seasonal mean (Karmakar et al. 2017a). Aerosols also can be a crucial factor in determining the rainfall patterns in intraseasonal timescale (Krishnamurti et al. 2013; Vinoj et al. 2014; Bhattacharya et al. 2016). Present study aims to understand some of the features ISO possess from an observational perspective and thus can be used to increase our knowledge on the possible changes in the nature of ISO. These results can also help in improving the short-to-medium range forecasting of rainfall over the Indian region.

Acknowledgements This work was supported by a research Grant from Ministry of Earth Sciences, Government of India (No. MM/SERP/FSUUSA/2013/INT-8-00) and NASA/PMM research Grant no. NNX16AD83G. We thank the anonymous reviewers for their constructive comments and suggestions.

References

Ajayamohan R, Merryfield WJ, Kharin VV (2010) Increasing trend of synoptic activity and its relationship with extreme rain events over central India. J Clim 23(4):1004–1013

Allen M, Robertson A (1996) Distinguishing modulated oscillations from coloured noise in multivariate datasets. Clim Dyn 12(11):775–784. https://doi.org/10.1007/s003820050142

Annamalai H, Slingo JM (2001) Active/break cycles: diagnosis of the intraseasonal variability of the Asian summer monsoon. Clim Dyn 18(1–2):85–102. https://doi.org/10.1007/s003820100161

Bhattacharya A, Chakraborty A, Venugopal V (2016) Role of aerosols in modulating cloud properties during active-break cycle of Indian summer monsoon. Clim Dyn 49:1–15

Chakraborty A, Nanjundiah RS (2012) Space-time scales of northward propagation of convection during boreal summer. Mon Weather Rev 140(12):3857–3866. https://doi.org/10.1175/MWR-D-12-00088.1

Dee D, Uppala S, Simmons A, Berrisford P, Poli P, Kobayashi S, Andrae U, Balmaseda M, Balsamo G, Bauer P et al (2011) The ERA-interim reanalysis: configuration and performance of the

data assimilation system. Q J R Meteorol Soc 137(656):553–597. https://doi.org/10.1002/qj.828
Ding R, Li J, Seo KH (2011) Estimate of the predictability of boreal summer and winter intraseasonal oscillations from observations. Mon Weather Rev 139(8):2421–2438
Gadgil S (2003) The Indian monsoon and its variability. Annu Rev Earth Planet Sci 31(1):429–467. https://doi.org/10.1146/annurev.earth.31.100901.141251
Ghil M, Allen M, Dettinger M, Ide K, Kondrashov D, Mann M, Robertson AW, Saunders A, Tian Y, Varadi F et al (2002) Advanced spectral methods for climatic time series. Rev Geophys 40(1):3-1–3-41. https://doi.org/10.1029/2000RG000092
Gill AE (1980) Some simple solutions for heat-induced tropical circulation. Q J R Meteorol Soc 106(449):447–462. https://doi.org/10.1002/qj.49710644905
Goswami BN, Ajayamohan RS, Xavier PK, Sengupta D (2003) Clustering of synoptic activity by Indian summer monsoon intraseasonal oscillations. Geophys Res Lett. https://doi.org/10.1029/2002GL016734
Goswami BN, Ajaya Mohan R (2001) Intraseasonal oscillations and interannual variability of the Indian summer monsoon. J Clim 14(6):1180–1198. https://doi.org/10.1175/1520-0442(2001)014%3c1180:IOAIVO%3e2.0.CO;2
Goswami B, Madhusoodanan M, Neema C, Sengupta D (2006) A physical mechanism for North Atlantic SST influence on the Indian summer monsoon. Geophys Res Lett 33(2):15
Hahn DG, Shukla J (1976) An apparent relationship between Eurasian snow cover and Indian monsoon rainfall. J Atmos Sci 33(12):2461–2462
Huffman GJ, Bolvin DT, Nelkin EJ, Wolff DB, Adler RF, Gu G, Hong Y, Bowman KP, Stocker EF (2007) The TRMM multisatellite precipitation analysis (TMPA): quasi-global, multiyear, combined-sensor precipitation estimates at fine scales. J Hydrometeorol 8(1):38–55. https://doi.org/10.1175/JHM560.1
Jiang X, Li T, Wang B (2004) Structures and mechanisms of the northward propagating boreal summer intraseasonal oscillation. J Clim 17(5):1022–1039. https://doi.org/10.1175/1520-0442(2004)017%3c1022:SAMOTN%3e2.0.CO;2
Julian P, Madden R (1981) Comments on a paper by T. Yasunari: a quasistationary appearance of 30-to 40-day period in the cloudiness fluctuations during the summer monsoon over India. J Meteorol Soc Jpn 59:435–437
Karmakar N, Chakraborty A, Nanjundiah RS (2017a) Increased sporadic extremes decrease the intraseasonal variability in the Indian summer monsoon rainfall. Sci Rep 7:7824. https://doi.org/10.1038/s41598-017-07529-6
Karmakar N, Chakraborty A, Nanjundiah RS (2017b) Space time evolution of the low- and high-frequency intraseasonal modes of the Indian summer monsoon. Mon Weather Rev 145(2):413–435. https://doi.org/10.1175/MWR-D-16-0075.1
Karmakar N, Chakraborty A, Nanjundiah RS (2015) Decreasing intensity of monsoon low-frequency intraseasonal variability over India. Environ Res Lett 10(5):054018. https://doi.org/10.1088/1748-9326/10/5/054018
Kemball-Cook S, Wang B (2001) Equatorial waves and air–sea interaction in the boreal summer intraseasonal oscillation. J Clim 14(13):2923–2942. https://doi.org/10.1175/1520-0442(2001)014
Krishnamurthy V, Ajayamohan RS (2010) Composite structure of monsoon low pressure systems and its relation to Indian rainfall. J Clim 23(16):4285–4305. https://doi.org/10.1175/2010JCLI2953.1
Krishnamurthy V, Shukla J (2007) Intraseasonal and seasonally persisting patterns of Indian monsoon rainfall. J Clim 20(1):3–20. https://doi.org/10.1175/JCLI3981.1
Krishnamurti TN, Subrahmanyam D (1982) The 30–50 day mode at 850 mb during MONEX. J Atmos Sci 39(9):2088–2095. https://doi.org/10.1175/1520-0469(1982)039%3c2088:TDMAMD%3e2.0.CO;2
Krishnamurti TN, Jayakumar P, Sheng J, Surgi N, Kumar A (1985) Divergent circulations on the 30 to 50 day time scale. J Atmos Sci 42(4):364–375. https://doi.org/10.1175/1520-0469(1985)042%3c0364:DCOTTD%3e2.0.CO;2
Krishnamurti TN, Martin A, Krishnamurti R, Simon A, Thomas A, Kumar V (2013) Impacts of enhanced CCN on the organization of convection and recent reduced counts of monsoon depressions. Clim Dyn 41(1):117–134. https://doi.org/10.1007/s00382-012-1638-z
Krishnamurti TN, Krishnamurti R, Das S, Kumar V, Jayakumar A, Simon A (2015) A pathway connecting the monsoonal heating to the rapid Arctic ice melt. J Atmos Sci 72(1):5–34. https://doi.org/10.1175/JAS-D-14-0004.1
Krishnan R, Zhang C, Sugi M (2000) Dynamics of breaks in the Indian summer monsoon. J Atmos Sci 57(9):1354–1372
Lau KM, Chan P (1986) Aspects of the 40–50 day oscillation during the northern summer as inferred from outgoing longwave radiation. Mon Weather Rev 114(7):1354–1367. https://doi.org/10.1175/1520-0493(1986)114%3c1354:AOTDOD%3e2.0.CO;2
Lee JY, Wang B, Wheeler MC, Fu X, Waliser DE, Kang IS (2013) Real-time multivariate indices for the boreal summer intraseasonal oscillation over the Asian summer monsoon region. Clim Dyn 40(1–2):493–509
Madden RA, Julian PR (1972) Description of global-scale circulation cells in the tropics with a 40–50 day period. J Atmos Sci 29(6):1109–1123
Moum JN, Pujiana K, Lien RC, Smyth WD (2016) Ocean feedback to pulses of the Madden–Julian Oscillation in the equatorial Indian Ocean. Nat Commun 7(13):203
Neelin JD, Held IM (1987) Modeling tropical convergence based on the moist static energy budget. Mon Weather Rev 115(1):3–12
Pai DS, Bhate J, Sreejith OP, Hatwar HR (2011) Impact of MJO on the intraseasonal variation of summer monsoon rainfall over India. Clim Dyn 36(1):41–55
Plaut G, Vautard R (1994) Spells of low-frequency oscillations and weather regimes in the Northern Hemisphere. J Atmos Sci 51(2):210–236. https://doi.org/10.1175/1520-0469(1994)051
Rajeevan M (2001) Prediction of Indian summer monsoon: status, problems and prospects. Curr Sci 81(11):1451–1458
Rajeevan M, Gadgil S, Bhate J (2010) Active and break spells of the Indian summer monsoon. J Earth Syst Sci 119(3):229–247. https://doi.org/10.1007/s12040-010-0019-4
Rajendran K, Kitoh A, Mizuta R, Sajani S, Nakazawa T (2008) High-resolution simulation of mean convection and its intraseasonal variability over the tropics in the MRI/JMA 20-km mesh AGCM. J Clim 21(15):3722–3739
Rasmusson EM, Carpenter TH (1983) The relationship between eastern equatorial Pacific sea surface temperatures and rainfall over India and Sri Lanka. Mon Weather Rev 111(3):517–528
Reynolds RW, Smith TM, Liu C, Chelton DB, Casey KS, Schlax MG (2007) Daily high-resolution-blended analyses for sea surface temperature. J Clim 20(22):5473–5496. https://doi.org/10.1175/2007JCLI1824.1
Seo KH, Schemm JKE, Wang W, Kumar A (2007) The boreal summer intraseasonal oscillation simulated in the NCEP climate forecast system: the effect of sea surface temperature. Mon Weather Rev 135(5):1807–1827. https://doi.org/10.1175/MWR3369.1
Sharmila S, Joseph S, Sahai A, Abhilash S, Chattopadhyay R (2015) Future projection of Indian summer monsoon variability under climate change scenario: an assessment from CMIP5 climate models. Glob Planet Chang 124:62–78
Sikka D, Gadgil S (1980) On the maximum cloud zone and the ITCZ over Indian, longitudes during the southwest monsoon. Mon

Weather Rev 108(11):1840–1853. https://doi.org/10.1175/1520-0493(1980)108%3c1840:OTMCZA%3e2.0.CO;2

Singh S, Kripalani R, Sikka D (1992) Interannual variability of the Madden–Julian oscillations in Indian summer monsoon rainfall. J Clim 5(9):973–978. https://doi.org/10.1175/1520-0442(1992)005%3c0973:IVOTMJ%3e2.0.CO;2

Sperber KR, Brankovic C, Deque M, Frederiksen C, Graham R, Kitoh A, Kobayashi C, Palmer T, Puri K, Tennant W et al (2001) Dynamical seasonal predictability of the Asian summer monsoon. Mon Weather Rev 129(9):2226–2248. https://doi.org/10.1175/1520-0493(2001)129%3c2226:DSPOTA%3e2.0.CO;2

Srinivasan J, Smith G (1996) The role of heat fluxes and moist static energy in tropical convergence zones. Mon Weather Rev 124(10):2089–2099

Subrahmanyam KV, Kumar KK, Narendra Babu A (2015) Phase relation between CAPE and precipitation at diurnal scales over the Indian summer monsoon region. Atmos Sci Lett 16(3):346–354

Turner AG, Annamalai H (2012) Climate change and the South Asian summer monsoon. Nat Clim Chang 2(8):587–595

Vinoj V, Rasch PJ, Wang H, Yoon JH, Ma PL, Landu K, Singh B (2014) Short-term modulation of Indian summer monsoon rainfall by West Asian dust. Nat Geosci 7(4):308–313

Wang B, Xie X (1997) A model for the boreal summer intraseasonal oscillation. J Atmos Sci 54(1):72–86

Webster PJ, Magaña VO, Palmer TN, Shukla J, Tomas RA, Yanai M, Yasunari T (1998) Monsoons: processes, predictability, and the prospects for prediction. J Geophys Res Oceans 103(C7):14451–14510. https://doi.org/10.1029/97JC02719

Wheeler MC, Hendon HH (2004) An all-season real-time multivariate MJO index: development of an index for monitoring and prediction. Mon Weather Rev 132(8):1917–1932

Xie X, Wang B (1996) Low-frequency equatorial waves in vertically sheared zonal flow. Part II: Unstable waves. J Atmos Sci 53(23):3589–3605

Yasunari T (1979) Cloudiness fluctuations associated with the Northern Hemisphere summer monsoon. J Meteorol Soc Jpn 57(3):227–242

Yasunari T (1980) A quasi-stationary appearance of 30 to 40 day period in the cloudiness fluctuations during the summer monsoon over India. J Meteorol Soc Jpn 58:225–229

Yoo JH, Robertson AW, Kang IS (2010) Analysis of intraseasonal and interannual variability of the Asian summer monsoon using a hidden Markov model. J Clim 23(20):5498–5516